A Monte Carlo Simulation of the High-Temperature Phases of Poly(*p*-hydroxybenzoic acid)

Stephen H. Foulger[†] and Gregory C. Rutledge*[,‡]

Department of Chemical Engineering, Massachusetts Institute of Technology, Cambridge, Massachusetts 02139

Received March 14, 1995; Revised Manuscript Received July 17, 1995[⊗]

ABSTRACT: The two high-temperature structures (identified as phase III and phase IV) of poly(*p*-hydroxybenzoic acid) (PHBA) are investigated through a molecular modeling methodology employing a Monte Carlo sampling of configurational phase space. Realistic chains of PHBA are represented by the explicit atom representation of the dimer repeat unit of the unit cell. States are sampled from the *NVT* ensemble using a scheme consisting of (1) valence angle and torsional angle variations and (2) rigid body rotations of the chain about the chain axis. Simulated X-ray diffraction data for the two phases are compared with experimental data from the literature. Intermolecular orientational probability density distributions indicate that phase III exhibits a wide range of intermolecular phenylene orientations, but with a retention of a herringbone-type packing in the $a-b$ plane. The phenylene rings of phase IV experience a greater intermolecular orientational freedom over phase III, but without free rotation. Intramolecular orientational probability density distributions indicate a preference for staggering the successive phenylene rings along the chain, with phase IV exhibiting a higher probability of the coplanar arrangement over that of phase III. The packing environments do not impose any severe restrictions on the torsion angles; the torsional angle populations of phases III and IV exhibited only minor variations relative to those exhibited by the individual chains free of interchain interactions.

1. Introduction

Stiff-chain polymers based on aromatic polyesters are currently of great scientific and industrial interest due to their superior solid-state properties. The monomer of *p*-hydroxybenzoic acid (HBA) is a basic constituent in a family of random copolyesters that exhibit thermotropic liquid crystalline behavior. Commercial molding or extrusion methods are unsuccessful in processing the homopolymer of HBA; this polymer (PHBA) is a highly crystalline, infusible, and intractable material. The copolyesters are generally comprised of a majority of HBA groups plus one or two comonomers to bring the processing temperature down to practical ranges. The structures of the homopolymer PHBA at high temperatures have been the subject of a number of investigations due to their close connection to the structural order in some copolyesters. The copolyesters with a majority of HBA residues often exhibit X-ray patterns very much like those of the high-temperature structures of PHBA. For this reason, the investigation of the high-temperature structures of PHBA is critical for the understanding of the structure–property relationships of a number of important copolyesters, yet the crystalline structure of PHBA is still the subject of debate.

At room temperature, two phases of the crystalline form of PHBA have been reported by various investigators using electron diffraction.[1,2] Phase I has an orthorhombic unit cell (a = 7.47–7.62 Å, b = 5.67–5.7 Å, c = 12.5–12.55 Å)[1–3] and is associated with polymeric HBA samples. It has been established that the c repeat distance corresponds to the length of a dimeric unit, and the lack of $00l$ reflections with l odd indicates the presence of a 2_1 screw axis parallel to the c-axis. While phase II is also orthorhombic (a = 11.06–11.12 Å, b = 3.77–3.78 Å, c = 12.89–12.9 Å),[2,4] it is observed in PHBA samples with low degrees of polymerization.

PHBA has been indicated to undergo two high-temperature phase transitions through investigations using methods of X-ray and electron diffraction, differential scanning calorimetry (DSC), and thermomechanical analysis (TMA). In the range 598–633 K,[5] both low-temperature phases convert to a phase III reportedly having a pseudohexagonal structure, since two dimer repeat units pack into an orthorhombic unit cell that exhibits hexagonal symmetry ($a \cong \sqrt{3}b$) on the $a-b$ plane. The cell parameters are a = 9.13–9.24 Å, b = 5.28–5.35 Å, and c = 12.49–12.5 Å.[1–3,6–9]

The sharp increase in the cell volume in going from phase I to phase III is due to the large increase in the a lattice parameter. This has been interpreted as being caused by an increasing rotational libration of the phenylene rings about their 1,4 axes, which have a preference of residing close to the (100) planes.[9] The periodicity along the chain changes insignificantly between phase I and phase III and is assumed to indicate a lack of a large-scale conformation reorientation of the chain. The structure of phase III has been proposed to exhibit some form of conformational disorder of the type observed in the smectic E phases of small rodlike molecules.[3,7] The chain conformation/packing models of phase III proposed by Yoon et al.[3] make it necessary to introduce a twofold axis of reorientation through 180° for each dimeric repeat unit around the chain axis. This proposed disorder was indicated to be a dynamic quantity by NMR and dielectric behavior studies at the elevated temperatures of phase III.[3,10]

The second high-temperature phase transition occurs at ca. 700 K and has been described as similar to a smectic E to smectic B transition of small rodlike molecules.[3,7] Phase III is transformed into a true hexagonal form (phase IV) with cell parameters of a = 9.31–9.35 Å, b = 5.36–5.40 Å, and c = 12.47–12.49 Å.[3] In the process of transforming from phase III to phase IV, the X-ray powder pattern is marked by the decrease of the 211 reflection while all other peaks maintain their intensities. From the results of dielectric studies, phase IV was suggested to have the same local packing

* To whom correspondence should be addressed.
[†] Department of Materials Science and Engineering.
[‡] Department of Chemical Engineering.
[⊗] Abstract published in *Advance ACS Abstracts,* September 1, 1995.

0024-9297/95/2228-7075$09.00/0

arrangement and chain conformation as phase III, with a loss of long-range orthorhombic coherence in the phenylene packing contributing to the 211 disappearance.[3]

The crystal structure of the two high-temperature phases of PHBA and the mechanism of the transitions between them are not yet fully clarified. The intent of this work is to analyze the proposed high-temperature structural models of PHBA in light of existing experimental and theoretical data through a molecular modeling methodology. For this work, a Monte Carlo (MC) model of the condensed phase of PHBA was chosen over molecular dynamics (MD) techniques to sample configuration phase space. MD techniques allow an assembly of atoms to evolve dynamically from their initial conditions under Newton's force law of interaction. To avoid high correlation of structure throughout the MD simulation, the duration of a run must be several multiples of the relaxation time of the slowest phenomenon being studied. NMR measurements[10] indicate that the phenylene rings have large-amplitude motion in the mid-kHz region in the low-temperature phases. Even allowing for several orders of magnitude increase in the frequency of these motions upon extrapolation to higher temperatures, these motions would still be well beyond the reach of state-of-the-art MD simulations. By contrast, Monte Carlo techniques generate the positions of the system in phase space stochastically. The MC trajectory can be viewed as an nth-order Markov chain, where the correlation of succeeding events can be tailored to maximize both model complexity and the search through phase space. This paper attempts to quantify the structural description and, in turn, the extent of order in PHBA through the Monte Carlo simulation of its high-temperature forms. Particular attention is focused on the effect of chain packing on the conformation of chains, as well as the relative intra- and intermolecular orientations of phenylene rings.

2. Model and Method

2.1. Force Field. The Monte Carlo simulations on the condensed phase of PHBA were performed on the basis of an explicit field presented by van Ruiten et al.[11] Full details of parameterization may be found there. Only a brief summary of the form and derivation is given here.

The force field consists of two-body nonbonded Lennard-Jones and Coulomb interactions (both depending on the distance r_{ij}), three-body bending potentials (depending on the valence angle θ_{ijk}), four-body dihedral potentials (depending on the torsional angle ϕ_{ijkl}), and four-body improper torsion potentials (depending on the improper torsion angle Φ_{ijkl}). The total system potential energy U is obtained by the summation over the appropriate combination of atoms over all chains:

$$U = \sum_{\text{chains}} \left\{ \sum_{ijk} U_{\text{valence},ijk} + \sum_{ijkl} U_{\text{torsion},ijkl} + \sum_{ijkl} U_{\text{improper torsion},ijkl} + \frac{1}{2}\sum_{ij} U_{\text{vdW},ij} + \frac{1}{2}\sum_{ij} U_{\text{Coulomb},ij} \right\} \quad (1)$$

where

$$U_{\text{valence},ijk} = \frac{1}{2}k_{\text{v}}(\theta_{ijk} - \theta_{ijk,0})^2 \quad (2)$$

$$U_{\text{torsion},ijkl} = \sum_{m=1}^{4} H_{m\phi}(1 - \cos(m\phi_{ijkl})) \quad (3)$$

$$U_{\text{improper torsion},ijkl} = H_{2\Phi}(1 - \cos(2\Phi_{ijkl})) \quad (4)$$

$$U_{\text{vdW},ij} = 4\epsilon_{ij}\left[\left(\frac{\sigma_{ij}}{r_{ij}}\right)^{12} - \left(\frac{\sigma_{ij}}{r_{ij}}\right)^{6}\right] \quad (5)$$

$$U_{\text{Coulomb},ij} = (4\pi\epsilon_0 r_{ij})^{-1} q_i q_j \quad (6)$$

All force constants k_{v}, $H_{m\phi}$, and $H_{2\Phi}$, the minimum energy valence angles $\theta_{ijk,0}$, the Lennard-Jones (LJ) parameters σ_{ij} and ϵ_{ij}, and the charges q_i are those from ref 11. The force field was parameterized on the basis of AM1 data of the dimers of HBA and 2-hydroxy-6-naphthoic acid (HNA). Considerable attention was paid to the accurate representation of the heights of the rotational barriers of the ester group torsions. These were obtained from AM1 calculations corrected by a 1.9 scaling factor.[12,13] Interactions between like atoms are those from the AMBER[14] force field, with the exception of the proximal carbonyl O−ring H interaction, as described in ref 11. The same LJ parameters have been used successfully to represent intermolecular interactions in molecular dynamics simulations of dimers and tetramers of *p*-hydroxybenzoic acid in the crystalline and nematic phases.[15,16]

The exact calculation of the long-range electrostatic interaction using the Ewald summation technique was deemed impractical for the long Monte Carlo simulations required here. Therefore, nonbonded interactions were considered only between nearest neighbor monomers, where the atom summation $(i-j)$ extended over net-neutral groups. The use of a neutral group cutoff prevented the artificial net accumulation of a residual electrostatic interaction at the cutoff boundary. For dispersion interactions, previous work has shown that the shell of nearest neighbors contains the dominant contribution to the energy that is responsible for the packing of the chains in the unit cell.[17,18]

2.2. Molecular Model. Each polymer chain comprises an explicit atom representation of the dimer repeat unit of the unit cell. The repeat unit of the polymer chain is illustrated in Figure 1. All atoms in the chain are treated as point centers of force for calculation of interaction energies. As stated earlier, all bond lengths and valence angles are held constant, with the exception of the five "backbone" angles of the ester group (labeled θ_1 through θ_5 in Figure 1). The phenylene rings are represented as rigid, hexagonal constructions of the ten bonded constituent atoms. The bonding at the trivalent carbonyl carbons in the ester group is fixed in the planar sp^2 hybridization configuration.

The experimental data indicate that the main changes between the crystal structures in the various phases of PHBA are due to the change in the packing of the phenylene rings orthogonal to the chain, while the chain conformation is generally believed to be unaffected. PHBA is a chain of alternating ester groups and *para*-linked phenylene rings. It is possible to rotate the phenylene moiety in PHBA without significantly altering the chain's conformation (see Figure 1), not unlike the aramid of poly(*p*-phenylene terephthalamide).[18] However, this rotation of the phenylene ring can have a drastic impact on the packing of the chains. Therefore, our model for PHBA consists of 16 chains (explicitly

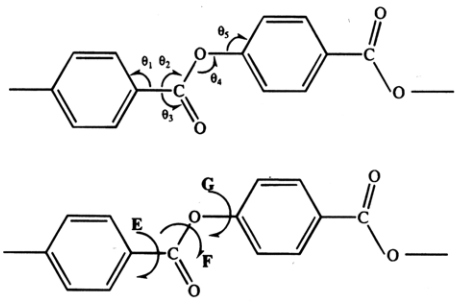

Figure 1. Segments of poly(*p*-hydroxybenzoic acid) (PHBA) with *cis* conformation. Valence angles (labeled θ_1 through θ_5) (upper) and torsions (labeled E, F, and G) (lower) of the ester group are indicated.

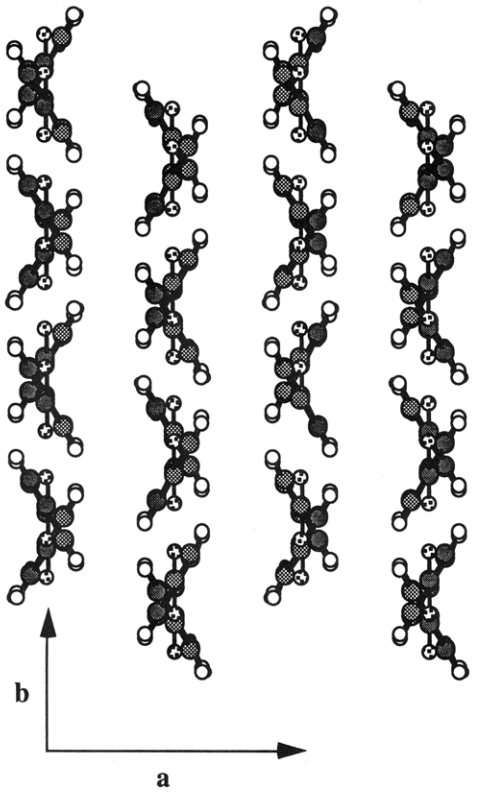

Figure 2. Initial configuration of simulation cell viewed along the *c*-axis. Carbons are designated as gray, hydrogens as white, and oxygens as speckled. The lattice translational vectors are indicated on the bottom.

represented by the dimer repeat unit) arrayed laterally to the *c*-axis to allow orientational flexibility in the layers of phenylene rings perpendicular to the chain axis (see Figures 2 and 3).

For the polar orientation of the chains in the unit cell, Lieser[2] proposed a $P2_12_12_1$ space group for phase I with two antiparallel chains along the *c*-axis, while Sun et al.[19] investigated various polarities of the chains in the unit cell for phase I without arriving at a definitive conclusion. For phase III, most crystallographic models have assumed a parallel orientation of the chains in the unit cell.[3,7] In this paper, the chains are placed on the lattice with a parallel polar orientation; i.e., the carbonyl bonds point in the same direction with respect to the *c* direction. The infinite chain is modeled by incorporating the bonding of each dimeric unit with its periodic image in the *c* direction, while the infinite system lateral to the chains is modeled by periodic boundary conditions.[20]

The initial chain conformations and relative chain orientations for both phase III and phase IV were based

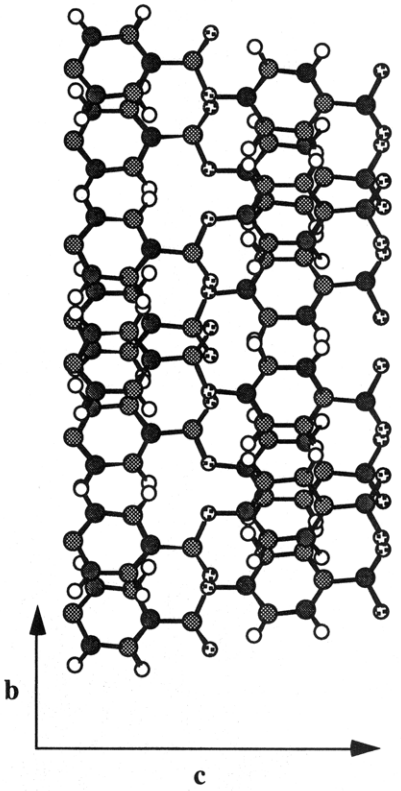

Figure 3. Initial configuration of simulation cell viewed along the *a*-axis. Atom designations are the same as in Figure 2. The lattice translational vectors are indicated on the bottom.

Table 1. Maximum Increments for Monte Carlo Sampling

variation	type	Δ (deg)
rigid body	—	8.0
torsion	E	2.0
	F	0.25
	G	3.0
valence	—	0.25

on the static model proposed by Yoon et al.[3] for the unit cell of the high-temperature form. The dimer repeat unit was placed in a 2_1 helix with the upper and lower phenylene rings staggered by 60°. The two dimer repeat units in the unit cell have their rings rotated in an opposite sense so as to give a herringbone packing of the phenylene rings in the $a-b$ plane when each chain is placed on the (experimentally determined) orthorhombic lattice. The geometric center of each molecule (x_{gc}, y_{gc}) was placed at the nodes of the $a-b$ basal plane, while the ester oxygen was assigned to reside in the $a-b$ plane. This procedure was used for both phase III (a = 9.23 Å, b = 5.27 Å, c = 12.50 Å) and phase IV (a = 9.35 Å, b = 5.40 Å, c = 12.46 Å) to give densities of 1.31 and 1.27 g/cm^3, respectively. Each dimer repeat unit was then subject to a random 180° rotation to account for the proposed reorientational disorder. The initial configuration for phase III and phase IV differ only in density.

The simulations sampled states from the *NVT* ensemble. The devised sampling scheme consisted of selecting uniformly distributed increments (δ) drawn from the range $-\Delta$ to $+\Delta$ (see Table 1) for (1) valence angles and torsional angles E, F, and G (see Figure 1) and (2) rigid body rotations of the dimer repeat unit around the chain axis (i.e., the *c* direction). For valence angles (θ) and torsional angles (ϕ), the old chain parameters were altered according to

$$\theta_{new} = \theta_{old} + \delta_{valence} \quad (7)$$

$$\phi_{new} = \phi_{old} + \delta_{torsion} \quad (8)$$

Rigid body rotations entailed spinning the chain around the c direction by $\delta_{rigid\ body}$. A Monte Carlo step consisted of either a full chain rebuild with valence angle and torsional angle variations or a rigid body rotation. Trial moves from an *old* chain configuration to a *new* chain configuration were selected or rejected according to a Metropolis importance criteria[21] of the change in the system's potential energy:

$$p = \min\left(1, \frac{\exp(-U_{new}/kT)}{\exp(-U_{old}/kT)}\right) \quad (9)$$

Chain rebuilds constituted 90% of all Monte Carlo steps. Within the rigid body rotations, 20% of the rotations were attempted 180° flips, while the remaining rotations were based on a smaller maximum increment. The maximum variation increments were chosen to produce a ca. 50% acceptance ratio.

Strong interactions between specific groups in adjacent polymer chains tend to introduce a preference for packing in layers composed of the interacting groups.[18] The fact that polyesters contain dipolar groups suggests that they may experience a similar packing. Crystallographic models of PHBA have stressed axial registration (i.e., phenylene next to phenylene and ester group next to ester group).[3,7] Therefore, displacements of the chain along the chain axis were not considered in this work. Pilot simulations which incorporated chain translations on the $a-b$ plane indicated that chain movement off the lattice nodes was negligible. This is in part due to the hexagonal packing ($a \cong \sqrt{3}b$) on the basal plane. We therefore have also neglected displacements of the chain within the $a-b$ plane.

For both condensed phases, the simulations were run for 5.0×10^6 Monte Carlo steps, with an equilibration period of 2.5×10^5 steps, averages being accumulated every 200 steps. Each system took 200 CPU hours running on an IBM RS/6000 37T. The temperature of the simulations was 608 K for phase III and 703 K for phase IV.

In addition to the condensed-phase simulations, Monte Carlo simulations were performed with the model system at the same temperature and density as the phase III and phase IV structures but without intermolecular interactions. The lack of intermolecular interactions allowed the individual chains to equilibrate free of neighbor interactions, thus describing "pseudorotator phases". These "phases" serve to establish reference points with which to compare the influence of the packing environment on the local structures. These simulations were run under the same equilibration and averaging conditions as the two condensed-phase runs.

2.3. X-ray Diffraction Calculations. The validation of this model was based on the X-ray scattering characteristics of the simulated phases and their correlation with experiment. For this purpose, unit cells of two dimers were identified within the simulation cell and the ensemble-averaged (indicated by the brackets $\langle\rangle$) structure factor was calculated in the usual manner:

$$\langle S_{hkl}\rangle = \frac{1}{Nn}\sum^{N}\sum^{n}\sum_{\alpha=1}^{\beta} f_\alpha[\exp(-2\pi i(hu_\alpha + kv_\alpha + lw_\alpha)] \quad (10)$$

where h, k and l are integers, N is the total number of times the simulation cell was sampled, n is the total number of unique unit cells in the simulation cell, β is the total number of atoms in the unit cell, and u_α, v_α, and w_α are the fractional coordinates of the α atom referenced to the unit cell. In this manner, $\langle S_{hkl}\rangle$ represents an average structure factor of the unit cells in the simulation cell, which itself is averaged over the entire simulation run. To compare the ensemble-averaged structure factor with the observed intensity I_{hkl}, the following corrections are necessary:[22]

$$\langle I_{hkl}\rangle = mpL|\langle S_{hkl}\rangle|^2 \quad (11)$$

where m is the multiplicity, p ($p = (1 + \cos^2 2\theta)/2$) is the polarization factor, and L ($L = (1/(\sin 2\theta \sin\theta))$ is the Lorentz factor. The maximum peak height was scaled to 100.0 with all other peaks scaled accordingly. The threshold intensity for consideration of significant peaks was 1% of the maximum peak intensity. The scattering angle 2θ is related to the scattered X-ray wavelength ($\lambda_{Cu\ K\alpha} = 1.5418$ Å) and to the distance of the lattice planes d by Bragg's law.

Powder diffraction patterns were simulated by convoluting the $\langle I_{hkl}\rangle$ peaks with a Gaussian distribution according to

$$I(2\theta) = c\sum_{hkl}\langle I_{hkl}\rangle\frac{1}{\sigma_{hkl}}\exp\left(-\left(\frac{4\ln(2)}{\sigma_{hkl}^2}\right)(2\theta - 2\theta_{hkl})^2\right) \quad (12)$$

where $2\theta_{hkl}$ is the position and σ_{hkl} is the full width at half-maximum (fwhm) of $\langle I_{hkl}\rangle$ and c is a scale factor. In this manner, each calculated intensity $\langle I_{hkl}\rangle$ is then proportional to the peak area.[23-25] The full width at half-maximum was set to 0.3° for the $00l$ peaks and 0.6° for all other peaks.[3]

2.4. Orientational Probability Density Distributions. Phenylene edge-to-face and carbonyl carbon-to-carbonyl oxygen interactions have been found to be dominant in a number of aromatic ester oligomer single crystals.[26] Previous investigators have attached a large significance to these phenylene interactions, and to a lesser degree the carbonyl interactions, in crystallographic models of the high-temperature phases.[7] To track these types of interactions, methods were devised to quantify (1) the relative intramolecular (conformational) ring orientation disorder, (2) the relative intermolecular ring orientation disorder (within a nearest neighbor shell), and (3) the intermolecular ring and ester group plane orientation disorder with respect to the fixed reference frame of the unit cell. For this purpose, each phenylene ring (i) was assigned a unit vector $\mathbf{v}_i$ that is copolanar with the ring and normal to the virtual bond spanning the phenylene moiety. The projection of $\mathbf{v}_i$ onto the $a-b$ plane (where $\mathbf{u}_a$ and $\mathbf{u}_b$ indicate the unit vectors in the a and b directions, respectively) gives a unit vector

$$\mathbf{v}_{ab,i} = \frac{((\mathbf{v}_i\cdot\mathbf{u}_a)\mathbf{u}_a + (\mathbf{v}_i\cdot\mathbf{u}_b)\mathbf{u}_b)}{\sqrt{(\mathbf{v}_i\cdot\mathbf{u}_a)^2 + (\mathbf{v}_i\cdot\mathbf{u}_b)^2}} \quad (13)$$

that indicates the orientation of the phenylene ring without regard to the tilt of the chain in the unit cell. With this vector, the angle

$$\theta_{ab,intra} = \cos^{-1}(\mathbf{v}_{ab,1}\cdot\mathbf{v}_{ab,2}) \quad (14)$$

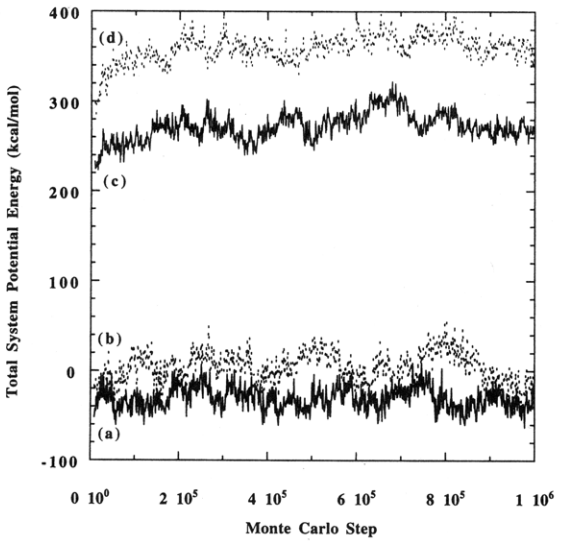

Figure 4. Total system potential energy plotted against the first 10^6 Monte Carlo steps for (a, —) smectic-E-like high-temperature phase III, (b, - - -) smectic-B-like high-temperature phase IV, (c, —) "pseudorotator phase III", and (d, - - -) "pseudorotator phase IV".

between the lower (1) and upper (2) phenylene rings of the dimer repeat unit can be calculated to reveal the intramolecular orientation of rings. The corresponding intermolecular orientation angle is calculated within a layer of phenylene rings between a ring (chain 1) and each ring (chain 2) in its nearest neighbor shell:

$$\theta_{ab,\text{inter}} = \cos^{-1}((\mathbf{v}_{ab,1})_{\text{chain 1}} \cdot (\mathbf{v}_{ab,1})_{\text{chain 2}}) \quad (15)$$

To quantify the orientation of the phenylene rings within the unit cell, the angle between the b lattice direction and $\mathbf{v}_{ab,i}$ is formed:

$$\psi_{ab,\text{ring}} = \cos^{-1}(\mathbf{v}_{ab,i} \cdot \mathbf{u}_b) \quad (16)$$

for each phenylene ring. The analogous angle

$$\psi_{ab,\text{carbonyl}} = \cos^{-1}(\mathbf{w}_{ab,i} \cdot \mathbf{u}_b) \quad (17)$$

between the b lattice direction and the $a-b$ plane projection $\mathbf{w}_{ab,i}$ of the unit vector defined by the carbonyl bond $\mathbf{w}_i$ is formed to indicate the orientation of the plane of the ester group within the unit cell.

3. Results and Discussion

The equilibration of the systems can be examined by observing the changes of the potential energy of the systems with the progression of the simulation. Figure 4 depicts the instantaneous total potential energy of each of the four systems with the first 1.0×10^6 Monte Carlo steps. Since each system was started from an array of perfectly ordered chains, the potential energy of each system equilibrated within 1.5×10^5 Monte Carlo steps, while the scattering characteristics of the system were slower in obtaining a steady average. The static model proposed by Yoon et al.[3] suggests that four unique orientations of the dimer repeat units in the unit cell contribute to $\langle S_{hkl} \rangle$ (eq 10). The slow convergence of the scattering characteristics in our simulations is due to the large conformational and rigid body reorientations of the dimer repeat units that are necessary to sample all of the atomic positions that contribute to $\langle S_{hkl} \rangle$. Pilot runs on the condensed phases indicted that the acceptance rate for 180° rigid body rotations was 1.5% for phase III and 2.1% for phase IV. We therefore chose 2.5×10^5 Monte Carlo steps (where 2% of the steps were devoted to attempted 180° rigid body rotations) for an equilibration period. At this point in the simulation, every chain in the system had statistically undergone 4.7 (phase III) and 6.6 (phase IV) 180° rigid body rotations. This equilibration period was considered sufficient to erase the influences of the initial configuration in the scattering averages. Figure 5 is a "snapshot" of the final configuration of the phase III simulation.

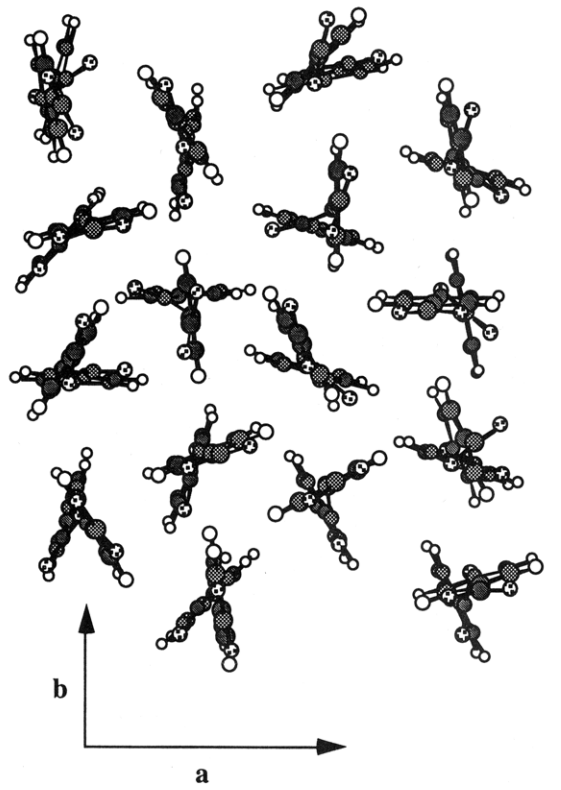

Figure 5. Final configuration of simulation cell of smectic-E-like high-temperature phase III viewed along the c-axis. Atom designations are the same as in Figure 2. The lattice translational vectors are indicated on the bottom.

Table 2. Average Relative X-ray Peak Intensities for Simulated Smectic-E-like High-Temperature Phase III

hkl	2θ (deg)	$\langle I_{hkl} \rangle$
002	14.1	1.8
004	28.5	3.5
006	43.4	4.9
110	19.3	100.0
111	20.6	1.3
116	47.9	2.1
200	19.2	55.5
206	47.9	1.4
211	26.6	16.6
213	33.5	3.8
310	33.7	3.9

An examination of the X-ray peak intensities for PHBA is appropriate to show that the simulated systems are representative of the physical material. Tables 2–5 list the average relative intensities for phase III, phase IV, "pseudorotator phase III", and "pseudorotator phase IV", respectively. The corresponding simulated powder diffraction patterns for the four systems appear in Figure 6, where the curves have been shifted vertically for clarity.

Table 6 is the comparison of integrated relative X-ray peak intensities for PHBA at 618 K taken from ref 3

Table 3. Average Relative X-ray Peak Intensities for Simulated Smectic-B-like High-Temperature Phase IV

hkl	2θ (deg)	$\langle I_{hkl} \rangle$
002	14.2	1.7
004	28.6	3.3
006	43.5	4.5
110	18.9	100.0
112	23.7	1.2
116	47.9	2.6
200	18.9	51.4
206	47.9	1.4
211	26.2	4.2
310	33.1	2.3

Table 4. Average Relative X-ray Peak Intensities for Simulated "Pseudorotator Phase III"

hkl	2θ (deg)	$\langle I_{hkl} \rangle$
002	14.1	2.7
004	28.5	4.9
006	43.4	6.8
110	19.3	100.0
116	47.9	2.5
200	19.2	51.4
206	47.9	1.3
310	33.7	2.0

Table 5. Average Relative X-ray Peak Intensities for Simulated "Pseudorotator Phase IV"

hkl	2θ (deg)	$\langle I_{hkl} \rangle$
002	14.2	2.3
004	28.7	4.1
006	43.6	5.5
110	19.0	100.0
116	47.9	2.4
200	19.0	48.5
206	47.9	1.1
310	33.2	1.7

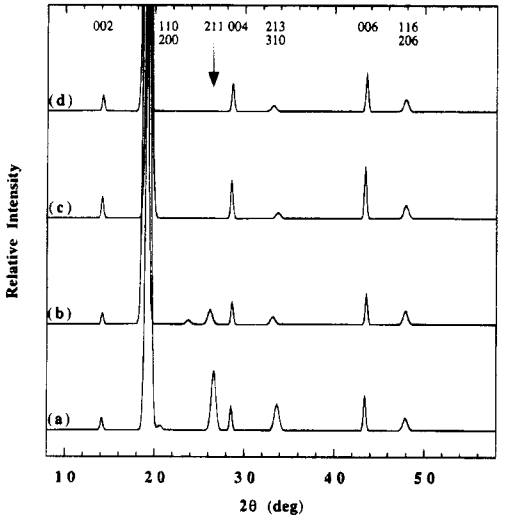

Figure 6. Simulated powder diffraction pattern for (a) smectic-E-like high-temperature phase III, (b) smectic-B-like high-temperature phase IV, (c) "pseudorotator phase III", and (d) "pseudorotator phase IV". The approximate position of the 211 peak is highlighted. The curves have been shifted vertically for clarity.

and the calculated average relative peak intensities for phase III (see also Figure 7). The simulated intensities for phase III are in good agreement with experimental data, though a few *hkl* ($h,k,l \neq 0$) reflections merit discussion. The *hkl* reflections in the condensed-phase simulations experienced the largest fluctuations throughout the runs, giving large standard deviations for their intensity averages. For example, the 211 peak had a standard deviation of ca. 25% of its intensity average.

Table 6. Comparison of Integrated Relative X-ray Peak Intensities for PHBA at 618 K Taken from Ref 3[a] and Average Relative X-ray Peak Intensities for Simulated Smectic-E-like High-Temperature Phase III at 608 K[b]

hkl	$2\theta^a$ (deg)	$I_{hkl}{}^a$	$2\theta^b$ (deg)	$\langle I_{hkl} \rangle^b$
002	14.2	1.0	14.1	1.2
004	28.5	1.6	28.5	2.3
006	43.4	1.8	43.4	3.2
110/200	19.4	100.0	19.3	100.0
111	—	—	20.6	1.3
116/206	47.8	0.9	47.9	2.3
211	26.6	8.2	26.6	10.7
213/310	33.6	1.5	33.6	4.9

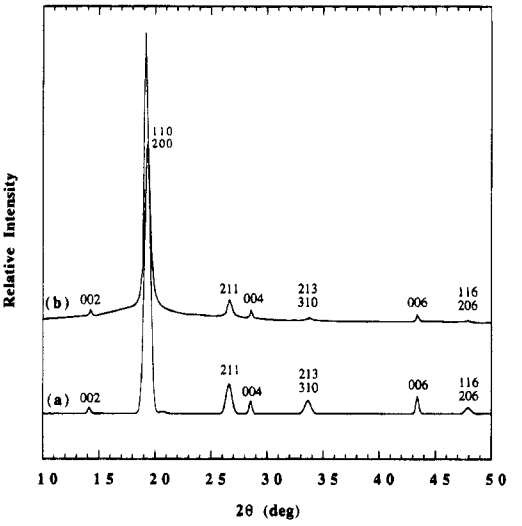

Figure 7. Comparison of simulated powder diffraction pattern for (a) smectic-E-like high-temperature phase III and (b) experimental data at 618 K taken from ref 3. The curves have been shifted vertically for clarity.

Thus, all of the *hkl* peak averages (within the statistical uncertainty of the simulation) compare favorably with experimental data. Also, the experimental data is 10° higher than simulation temperature and could manifest itself as a slight reduction of the *hkl* reflections of the experimental data over the calculated data. The appearance of the 111 reflection in phase III is surprising, yet its small height and its close proximity to the 110/200 reflections make it unclear if it is present in the experimental data. The average intensity of the simulated 211 and 213 reflections is more intense than the experimental data and an additional possible source for this discrepancy is found in the use of a parallel polar orientation of the chains in the unit cells. Coulter et al.[7] found that crystallographic models of phase III with the parallel orientation tended to overpredict the intensities of the 002, 211, and 213 reflections, while a random assignment of polar orientations of the chains in the unit cells predicted these reflections to be too weak. It was suggested that phase III possibly consists of a mixture of the two crystal forms.

The simulated phase IV X-ray peak intensities are similar in height to those of the peaks of phase III, with the majority of reflections experiencing a slight decrease in relative height. The greatest reduction was in the peak height of the 211 reflection (see Table 3). This reduction of the 211 peak is in accordance with experimental data.[3,7,9] The appearance of the 112 reflection is not observed in the experimental data. Due to its small intensity and its absence in the phase III and both "pseudorotator phases" reflections, we feel that the appearance of this peak is due to statistical uncertainty of the simulation. Nonetheless, the general agreement

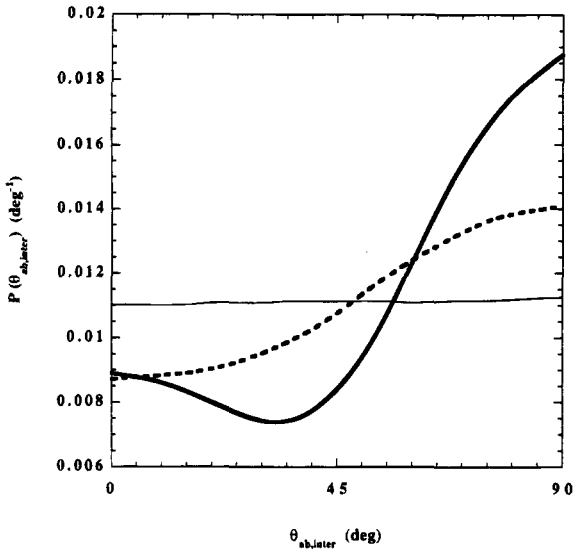

Figure 8. Probability density distribution of $\theta_{ab,\text{inter}}$ for smectic-E-like high-temperature phase III (bold —), smectic-B-like high-temperature phase IV (bold - - -), and "pseudorotator phase III" (—). The "pseudorotator phase IV" curve is omitted for clarity; see text for details. The plotted range is 0–90° due to the bilateral symmetry of the phenylene ring.

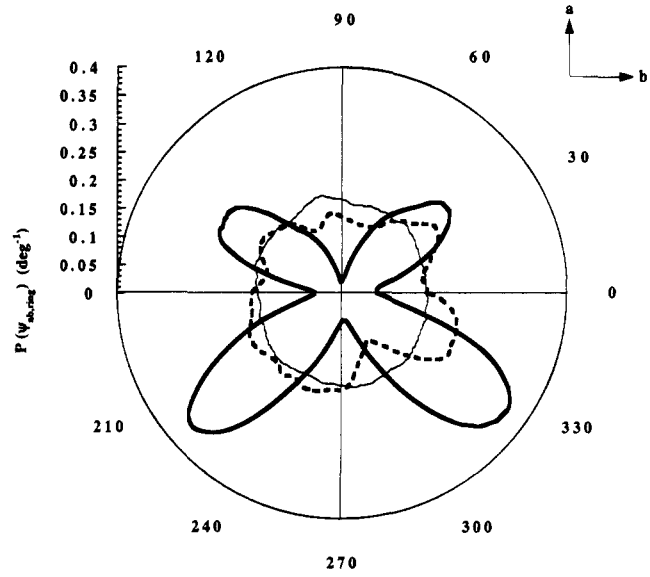

Figure 9. Probability density distribution of $\psi_{ab,\text{ring}}$ for smectic-E-like high-temperature phase III (bold —), smectic-B-like high-temperature phase IV (bold - - -), and "pseudorotator phase III" (—). The "pseudorotator phase IV" curve is omitted for clarity; see text for details. 0° corresponds to the b direction.

of the model systems with experimental diffraction results indicates that they are representative of phase III and phase IV.

The reduction in intensity of the 211 reflection in transforming from phase III to phase IV has been attributed to a loss in the long-range orthorhombic coherence in the phenylene ring packing. The coherence of each phenylene and its layer shell of nearest neighbor rings can be quantified by the probability density distribution of $\theta_{ab,\text{inter}}$ (eq 15) (see Figure 8). In the initial phenylene herringbone-type packing, the distribution of $\theta_{ab,\text{inter}}$ has, with regard to a phenylene ring centered at fractional coordinates [0,0] in the $a-b$ projection, four contributions of 60° from phenylene rings located at [±1/2,±1/2] and two contributions of 0° from phenylene rings located at [0,±1]. In all four simulations, those initial spikes rapidly equilibrated to fairly smooth distributions. As expected, the extreme cases of both "pseudorotator phases" gave uniform probability density distributions of ring–ring orientations due to the lack of interchain correlations; thus only "pseudorotator phase III" is plotted in Figure 8 for clarity. Phase III has two broad maximum populations of inter-ring orientations in its distribution, one centered about 0° and the other about 90°, and a clear minimum at ca. 35°. The phenylene rings of phase III are sampling a wide range of intermolecular orientations, but the basic herringbone-type packing in the $a-b$ plane is retained with the two pairs of phenylene rings in the unit cell maintaining an edge to face orientation.

The probability density distribution of intermolecular phenylene orientations of phase IV is much more uniform than that of phase III. The curve is characterized by a broad maximum centered at 90°. The minimum at ca. 35° has essentially disappeared. The phenylene rings of phase IV experience a greater intermolecular orientational freedom over phase III, but with the same retention of preference for the phenylene edge to face orientation. This orientational freedom suggests a reduced intermolecular confinement of the phenylene rings. Lukasheva et al.[27] have performed configuration space scans of the intermolecular potential energy in layers of phenylene rings perpendicular to the chain axis for both phase III and IV that indicate that the path between potential energy minima of phase IV has widened over that of phase III, leading to less restrictive orientations of the phenylene rings. This increased phenylene ring freedom is consistent with a loss in the orthorhombic coherence in the phenylene packing as proposed by Yoon et al.[3]

A measure of the influence of the packing environment on the local structure can be revealed by comparing the probability density distributions of various intra- and intermolecular orientations of the phenylene moieties and ester groups in the two condensed phases with the "pseudorotator phases". The probability density distribution of $\psi_{ab,\text{ring}}$ (eq 16) for phase III, phase IV, and "pseudorotator phase III" are depicted in polar form in Figure 9. Again, the results of both "pseudorotator phases" were identical and only "pseudorotator phase III" is plotted in Figure 9 for clarity. In this plot, 0° corresponds to the b direction and 90° corresponds to the a direction. The probability density is plotted radially. The highest probabilities appear as lobes centered around four orientational sites at ca. 40, 140, 220, and 320° for phase III, while the "pseudorotator phases" populate all orientations uniformly. Phase IV has only remnants of the four orientational lobes; the distribution is very similar to a uniform distribution. Table 7 lists the average and standard deviation of $\psi_{ab,\text{ring}}$ as well as those of $\psi_{ab,\text{carbonyl}}$ with respect to the $b-c$ plane, averaged over the four quadrants. The rings, on average, are rotated 40° from the $b-c$ plane for phase III, while the more open structure of phase IV allows the phenylene rings to rotate out to 43°. The reduced standard deviation of this rotation from the $b-c$ plane for phase III over that of phase IV suggests that the phenylene rings are more restricted to these orientations in phase III.

To summarize the intermolecular ring orientational results, the density distributions of $\theta_{ab,\text{inter}}$ in our high-temperature simulations lead to a picture of layers of phenylene rings packing with a preference for edge to face orientations for both phases while the distributions of $\psi_{ab,\text{ring}}$ indicate that the placement of the rings within

Table 7. First Two Moments of the Probability Density Distributions of $\psi_{ab,ring}$ and $\psi_{ab,carbonyl}$ Referenced from the $b-c$ Plane for Smectic-E-like High-Temperature Phase III, Smectic-B-like High-Temperature Phase IV, and "Pseudorotator Phases"[a]

phase III		phase IV		"pseudorotator phases"	
$\bar{\psi}_{ab,ring}$	σ	$\bar{\psi}_{ab,ring}$	σ	$\bar{\psi}_{ab,ring}$	σ
40	18	43	25	45	25
phase III		phase IV		"pseudorotator phases"	
$\bar{\psi}_{ab,carbonyl}$	σ	$\bar{\psi}_{ab,carbonyl}$	σ	$\bar{\psi}_{ab,carbonyl}$	σ
42	22	43	25	45	25

[a] A uniform distribution gives $\bar{\psi}_{theoretical} = 45.0°$ and $\sigma_{theoretical} = 25.98°$. All listed values are in degrees.

the unit cell becomes much less restrictive in going from phase III to phase IV. In phase III, the phenylene rings are preferentially placed roughly ca. ±40° out of the $b-c$ plane, with a large variance in this angle. Thus, the intermolecular phenylene ring angle between the [0,0] and [$^1/_2$,$^1/_2$] ring is expected to be about 80°, but due to a correlation in the arrangement of the two rings, a stricter edge to face orientation of ca. 90° is maintained. This is in contrast to minimum potential energy calculations of phase I[27] and experimental single-crystal X-ray diffraction studies of monodisperse aromatic oligomers[26] that indicate that the intermolecular phenylene ring angle generally falls within the range of 40–70° for packed aromatic structures at *low* temperatures. Our results indicating a higher inter-ring angle are in accordance with minimum potential energy calculations[27] of phase III and phase IV where the minimum energy configuration placed the phenylene ring at ca. 40° out of the $b-c$ plane, giving an inter-ring angle of ca. 80°. In addition, the results of fitting crystallographic models[7] for phase III to X-ray data indicate that the chain geometry must be altered from minimum potential energy conformations. When packed on a lattice, the minimum intramolecular energy conformer gave an intermolecular phenylene ring angle of 60°. Fitting to data required the rotation of the phenylene rings out toward 90° (e.g., see endnote of ref 7). Evidently, the increase in temperature leads to libration of the phenylene rings around their 1,4 axis, rotating them out to higher angles than predicted solely by intramolecular minimum energy arguments.

The probability density distribution of the corresponding angle $\psi_{ab,carbonyl}$ (eq 17) (i.e., the plane of the ester group) for phase III, phase IV, the "pseudorotator phase III" is depicted in Figure 10. This plot indicates that the carbonyl bond also roughly populates the same four orientational sites as the phenylene planes in phase III, but with a greater variance (see Table 7). This is not surprising since intramolecular potential energy calculations of torsion E indicate that the carbonyl and phenylene ring prefer to remain planar with a conformational energy barrier of ca. 5 kcal/mol[11,28–30] and the total intermolecular energy around the minimum does not preclude a planar form.[27] The curve of phase IV appears to be very close in form to the uniform curve of the "pseudorotator phases", with only a slightly higher probability of the ester plane populating one of the four sites.

The probability density distribution of $\theta_{ab,intra}$ (eq 14) for phase III, phase IV, "pseudorotator phase III", and "pseudorotator phase IV" is depicted in Figure 11. The majority of the populations are located between 45 and 90°, which indicates that the dimer repeat unit of the

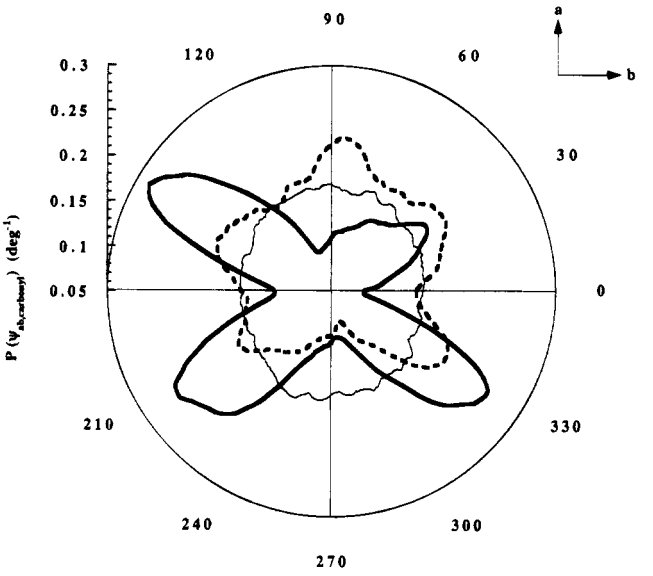

Figure 10. Probability density distribution of $\psi_{ab,carbonyl}$ for smectic-E-like high-temperature phase III (bold —), smectic-B-like high-temperature phase IV (bold - - -), and "pseudorotator phase III" (—). The "pseudorotator phase IV" curve is omitted for clarity; see text for details. 0° corresponds to the b direction.

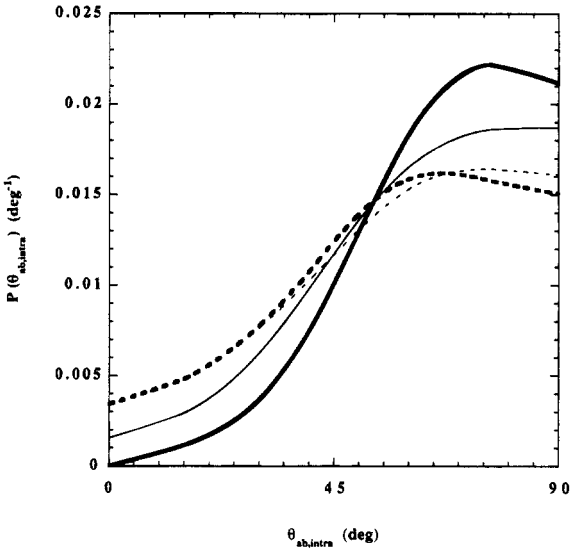

Figure 11. Probability density distribution of $\theta_{ab,intra}$ for smectic-E-like high-temperature phase III (bold —), smectic-B-like high-temperature phase IV (bold - - -), "pseudorotator phase III" (—), and "pseudorotator phase IV" (- - -). The plotted range is 0–90° due to the bilateral symmetry of the phenylene ring.

unit cell prefers to place its phenylene rings in a staggered arrangement for all four simulations. Minimum energy conformations of the dimer place the rings at a staggering of ca. 45°, but with increasing temperature, the "thermalization" of the torsions allows the rings to increase the staggering angle significantly. The packing environment of phase III appears to accentuate the population of rings staggered by 75–80° in comparison to "pseudorotator phase III". By contrast, the environment in phase IV has no major effect in comparison to "pseudorotator phase IV", yet the population of rings staggered at low angles for phase IV is greatly increased relative to phase III.

A further measure of the influence of the packing environment on the local structure can be revealed by comparing the probability density distributions of the

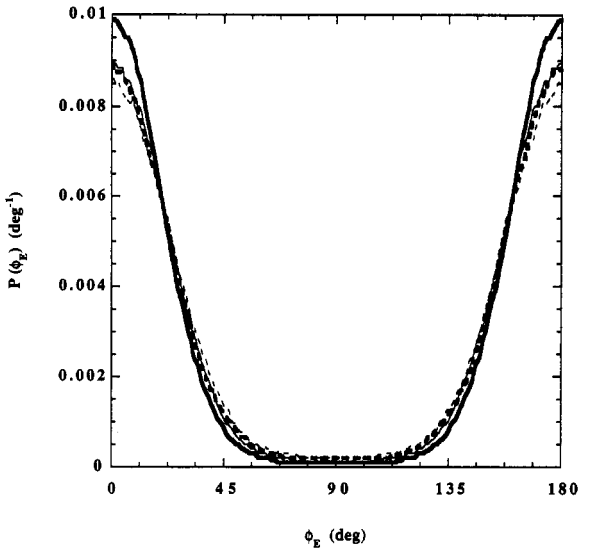

Figure 12. Probability density distribution of torsion E for smectic-E-like high-temperature phase III (bold —), smectic-B-like high-temperature phase IV (bold - - -), "pseudorotator phase III" (—), and "pseudorotator phase IV" (- - -). Only half of the total torsional range is plotted for clarity.

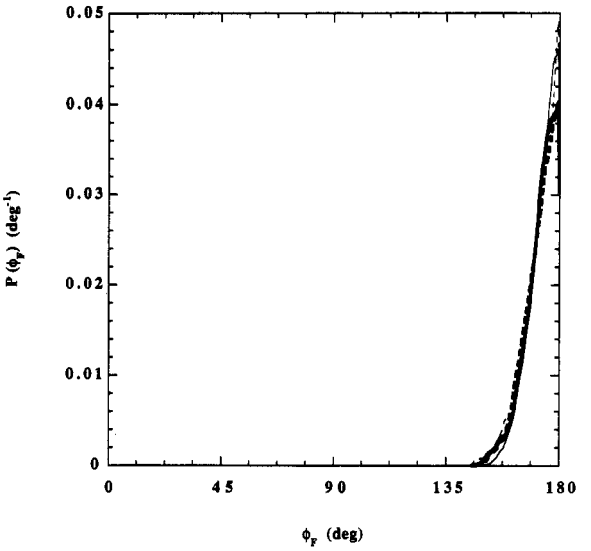

Figure 13. Probability density distribution of torsion F for smectic-E-like high-temperature phase III (bold —), smectic-B-like high-temperature phase IV (bold - - -), "pseudorotator phase III" (—), and "pseudorotator phase IV" (- - -). Only half of the total torsional range is plotted for clarity.

torsional angles of the ester group in the two condensed phases with the "pseudorotator phases". The changes in these torsional probability density distributions are slight between the four simulations. The torsional probability density distribution of torsion E for the four simulations is depicted in Figure 12. This plot corroborates the high probability of placement of the carbonyl in the same plane as the phenylene ring for phase III (see Figures 9 and 10). Phase III shows an increased probability for torsional angles at 0 and 180° over phase IV and the "pseudorotator phases", while the curves almost superimpose for these latter three cases. The increased probability of planar conformations of the ester group and the phenylene moiety in phase III over "pseudorotator phase III" must be attributed to the packing environment.

The torsional probability density distributions of torsions F and G for phase III, phase IV, and both "pseudorotator phases" are depicted in Figures 13 and 14. Torsion F of phase III and IV shows a decreased probability for torsional angles at 180° from that of the "pseudorotator phases". Of the three torsions, E, F, and G, the major component in determining the intramolecular phenylene ring staggering is torsion G. The probability density distribution of torsion G has a slightly decreased probability at 0 and 180° for phase III with respect to the "pseudorotator phases", while the curves of phase IV and "pseudorotator phase IV" almost superimpose at these angles. Phase IV has an increased probability at 0 and 180° relative to phase III. This is consistent with the probability density distribution of $\theta_{ab,\text{intra}}$ (see Figure 11) where there is a higher probability of a coplanar ring arrangement for phase IV over phase III.

Obviously, the packing environment does not impose a great hindrance for any of the torsions E–G, yet the concerted variations in these "thermalized" torsions allows the minimum energy intraphenylene ring angle of 45° to open up to greater angles. This lack of environmental influence on the independent torsional distributions was also seen in molecular dynamics simulation results of dimers and tetramers of *p*-hydroxybenzoic acid in the liquid crystalline state.[16]

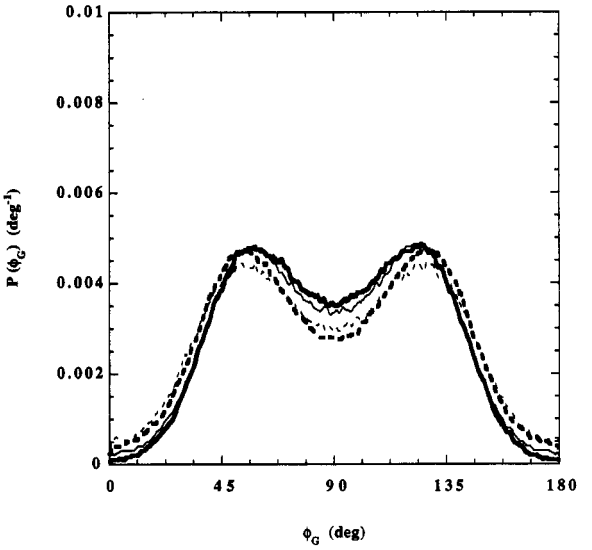

Figure 14. Probability density distribution of torsion G for smectic-E-like high-temperature phase III (bold —), smectic-B-like high-temperature phase IV (bold - - -), "pseudorotator phase III" (—), and "pseudorotator phase IV" (- - -). Only half of the total torsional range is plotted for clarity.

4. Conclusion

The two high-temperature structures (identified as phase III and phase IV) of poly(*p*-hydroxybenzoic acid) (PHBA) are investigated through a molecular modeling methodology employing a Monte Carlo sampling of configurational phase space. Realistic chains of PHBA are represented by the explicit atom representation of the dimer repeat unit of the unit cell. States are sampled from the *NVT* ensemble using a sampling scheme consisting of (1) valence and torsional variations and (2) rigid body rotations of the chain about the chain axis. Simulated X-ray diffraction data for the two phases are compared with experimental data from the literature. The intensity of the 211 reflection decreased in phase IV with respect to phase III, consistent with experimental results.

Intermolecular orientational probability density distributions indicate that phase III exhibits a wide range

of intermolecular phenylene orientations, but with a retention of a herringbone-type packing in the $a-b$ plane. The phenylene rings, on average, are rotated ca. 40° from the $b-c$ plane for phase III. The phenylene rings of phase IV experience a greater intermolecular orientational freedom over phase III, but without free rotation. The two pairs of phenylene rings in the unit cell maintain an edge to face orientation. This is consistent with a loss in the orthorhombic coherence in the phenylene packing as proposed by Yoon et al.[3]

Intramolecular orientational probability density distributions indicate a preference for staggering the successive phenylene rings along the chain, with phase IV having a higher probability of exhibiting the coplanar arrangement over that of phase III. The packing environments do not impose any severe restrictions on the torsion angles; the torsional angle populations of phases III and IV exhibited only minor variations as compared to an intermolecular interaction-free "pseudorotator phase".

Acknowledgment. We want to thank Dr. D. Y. Yoon for kindly supplying us with the experimental X-ray diffraction data and Prof. D. Lacks of Tulane University for helpful discussions. We are also grateful to E. I. du Pont de Nemours, Inc., for financial support through a Young Faculty Award to G.C.R. and to the Center for High Performance Computing at Washington University for a generous allocation of computer time.

References and Notes

(1) Geiss, R.; Volksen, W.; Tsay, J.; Economy, J. *J. Polym. Sci., Polym. Lett. Ed.* **1984**, *22*, 433.
(2) Lieser, G. J. *J. Polym. Sci., Polym. Phys. Ed.* **1983**, *21*, 1611.
(3) Yoon, D. Y.; Masciocchi, N.; Depero, L. E.; Viney, C.; Parrish, W. *Macromolecules* **1990**, *23*, 1793.
(4) Liu, J.; Geil, P. H. *J. Macromol. Sci., Phys.* **1992**, *B31*, 163.
(5) Economy, J.; Stern, R. S.; Matkovich, V. I.; Cottis, S. G.; Nowak, B. E. *J. Polym. Sci., Polym. Chem. Ed.* **1976**, *14*, 2207.
(6) Blackwell, J.; Lieser, G.; Gutierrez, G. A. *Macromolecules* **1983**, *16*, 1418.
(7) Coulter, P.; Hanna, S.; Windle, A. H. *Liq. Cryst.* **1989**, *5*, 1603.
(8) Economy, J.; Volksen, W.; Viney, C.; Geiss, R.; Siemens, R.; Karis, T. *Macromolecules* **1988**, *21*, 2777.
(9) Hanna, S.; Windle, A. H. *Polym. Commun.* **1988**, *29*, 236.
(10) Lyerla, J. R.; Economy, J. E.; Maresch, G. G.; Muhlebach, A.; Yannoni, C. *Liquid Crystal Polymers*; American Chemical Society: Washington, DC, 1990.
(11) van Ruiten, J.; Meier, R. J.; Hahn, C.; Mosell, T.; Sariban, A.; Brickmann, J. *Macromolecules* **1993**, *26*, 1555.
(12) Fabian, W. *J. Comput. Chem.* **1988**, *9*, 369.
(13) Coussens, B.; Pierloot, K.; Meier, R. J. *J. Mol. Struct. Theochem* **1992**, *259*, 331.
(14) Weiner, S. J.; Kollman, P. A.; Nguyen, D. T.; Case, D. A. *J. Comput. Chem.* **1986**, *7*, 230.
(15) Jung, B.; Schürmann, B. L. *Mol. Cryst. Liq. Cryst.* **1990**, *185*, 141.
(16) Huth, J.; Mosell, T.; Nicklas, K.; Sariban, A.; Brickmann, J. *J. Phys. Chem.* **1994**, *98*, 7685.
(17) Tripathy, S. K.; Hopfinger, A. J. *J. Phys. Chem.* **1981**, *85*, 1371.
(18) Rutledge, G. C.; Suter, U. W. *Macromolecules* **1991**, *24*, 1921.
(19) Sun, Z.; Cheng, H. M.; Blackwell, J. *Macromolecules* **1991**, *24*, 4162.
(20) Allen, M. P.; Tildesley, D. J. *Computer Simulation of Liquids*; Oxford University Press: New York, 1987.
(21) Metropolis, N.; Rosenbluth, A. W.; Rosenbluth, M. N.; Teller, A. H.; Teller, E. *J. Chem. Phys.* **1953**, *21*, 1087.
(22) Warren, B. E. *X-Ray Diffraction*; Dover Publications, Inc.: New York, 1990.
(23) Rietveld, H. M. *Acta Crystallogr.* **1966**, *20*, 508.
(24) Rietveld, H. M. *Acta Crystallogr.* **1967**, *22*, 151.
(25) Rietveld, H. M. *J. Appl. Crystallogr.* **1969**, *2*, 65.
(26) O'Mahony, C.; Williams, D.; Colquhoun, H.; Blundell, D. *Polymer* **1990**, *31*, 1603.
(27) Lukasheva, N. V.; Sariban, A.; Mosell, T.; Brickmann, J. *Macromolecules* **1994**, *27*, 4726.
(28) Sun, H. *J. Comput. Chem.* **1994**, *15*, 752.
(29) Hummel, J. P.; Flory, P. J. *Macromolecules* **1980**, *13*, 479.
(30) Coulter, P.; Windle, A. H. *Macromolecules* **1989**, *22*, 1129.

MA950349K